This article has been accepted for publication in IEEE Access. This is the author's version which has not been fully edited and content may change prior to final publication. Citation information: DOI 10.1109/ACCESS.2025.3531956

IEEE Access
Multidisciplinary | Rapid Review | Open Access Journal

Date of publication xxxx 00, 0000, date of current version xxxx 00, 0000.

Digital Object Identifier 10.1109/ACCESS.2024.0429000

A 3D-Printed Spherical Dual-Circular Polarized Luneburg Lens Antenna for Ku-Band

QING WANG[1], XIAOHAI HAN[1], PU YU[2], JIAN-QIANG HOU[1], AND ZHEN-YA LEI[1]
[1]School of Electronic Engineering, Xidian University, Xi'an 710071, China
[2]Shaanxi Changling Electronic Technology Co., Ltd, Xi'an 710117, China

Corresponding author: Xiaohai Han (e-mail: xduhxh@163.com).

This work was supported in part by Provincial Science Foundation of Shaanxi (2021JM-128).

ABSTRACT In this paper, we propose a novel three-dimensional-printed Luneburg lens for converting linear polarization to dual-circular polarization and successfully apply it in a multibeam antenna. The discrete unit cell, used as the gradient-index material to approximate the required refractive index in the Luneburg lens, has its effective refractive index calculated by effective medium theory. To achieve the polarization conversion, the symmetry of the unit cell is disrupted. A 100 mm diameter lens is designed to operate at 12.6-17.1 GHz, fed by a low-profile dual-polarized magneto-electric dipole antenna. By analyzing the size and isolation of the antenna, a multibeam lens antenna with five feeds was designed, which features a compact antenna layout and low coupling between them. The multibeam Luneburg lens antenna enables beam scanning of $\pm 60^{\circ}$ in the horizontal plane. Measurement results show an overlapped bandwidth of 30% with reflection coefficients below -10 dB and axial ratios under 3 dB. At the center frequency of 15 GHz, the gain reaches 21 dBi, approximately 14 dB higher than the magneto-electric dipole antenna without the lens.

INDEX TERMS Dual-circular polarization antenna, Luneburg lens, multibeam antenna, polarization conversion, three-dimensional-printed antenna.

I. INTRODUCTION

IN the field of modern communication technology, the performance of antenna systems is crucial. Antennas with multibeam [1]–[3], wide-angle scanning [4]–[6] and high gain [7]–[9], are highly sought after. To meet these requirements, various types of antennas have been studied and developed, including phased array antennas [10], [11], reflector antennas [12], [13], and lens antennas [14], [15]. Phased array antennas are based on electrically controlled scanning, which achieves precise beam control by adjusting the amplitude and phase of each element. However, their feeding network is too complex and costly [16]. Reflector antenna have simple structures, but they are not easy to achieve beam scanning [17]. Lens antennas offer advantages such as ease of manufacture, small size, and low cost. As a result, lens antennas have found wide applications in satellite communication, radar systems, and millimeter waves.

One example of a spherical lens antenna is the Luneburg lens, which was proposed in 1944 and is a classic gradient-index lens [18]. Unlike constant refractive index lenses, gradient refractive index lenses are easier to use for beam regulation. However, due to the inability to achieve continuously varying refractive indices, there were no reports on the Luneburg lens for a long time. Later on, traditional layering techniques were proposed to discretize continuous refractive indices and approximate varying refractive indices using multi-layer structures [19]–[21]. However, these methods resulted in significant losses due to the gaps between each layer. Good manufacturing processes can help improve these issues but also increase costs. With advancements in material manufacturing processes, variable refractive indices can now be achieved by drilling holes or adding columns to the substrate [22]–[27] or by printing metal patterns on a printed circuit board [28]–[30]. However, it is worth noting that most of the designed Luneburg lens using these methods are two-dimensional (2D).

In recent years, the advancement of three-dimensional-printing (3DP) technology has provided a cost-effective approach to fabricating intricate three-dimensional (3D) structures. This technology has found significant application in the production of metamaterials, particularly in the development of metamaterial Luneburg lens [31]–[35]. Previous studies have utilized 3DP to manufacture Luneburg lenses by discretizing them into smaller units and modifying the dielectric filling rate of these units to control the equivalent refractive index. This approach enables precise control over the refrac-

This work is licensed under a Creative Commons Attribution-NonCommercial-NoDerivatives 4.0 License. For more information, see https://creativecommons.org/licenses/by-nc-nd/4

This article has been accepted for publication in IEEE Access. This is the author's version which has not been fully edited and
content may change prior to final publication. Citation information: DOI 10.1109/ACCESS.2025.3531956

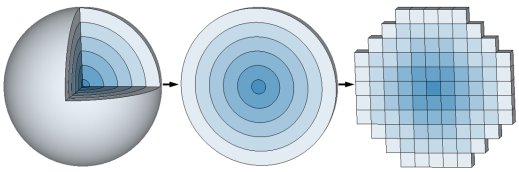

FIGURE 1. The process of discretizing an ideal Luneburg lens into multiple unit cells.

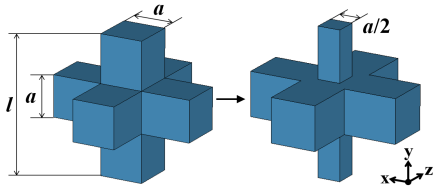

FIGURE 2. The geometry of the unit cell and disrupting the symmetry of the unit cell.

tive index at different positions of the lens, approximating a continuously varying refractive index. However, most existing reports highlight the dependence of the Luneburg lens antenna's polarization on the feed source.

This paper introduces a novel 3D-printed Luneburg lens that achieves the conversion from linear polarization to dual-circular polarization. There are several innovation points of our Luneburg lens.

(1) Asymmetric crisscross unit cells were used to obtain polarization conversion function, which is convenient to manufacture and has a stable structure.

(2) It can achieve the conversion from dual-linear polarization to dual-circular polarization.

(3) The polarization mode can be easily changed by switching the port of the feeding antenna instead of mechanical rotation.

The proposed lens antenna retains its original excellent characteristics while adding polarization conversion function to the traditional Luneburg lens. By breaking the symmetry of metamaterial unit cells, different propagation characteristics for horizontally and vertically polarized electromagnetic waves are achieved [35]. Consequently, this lens can convert linearly polarized waves to circularly polarized waves. The lens offers several advantages, including high gain, wide bandwidth, and low cost. Additionally, it can be utilized in multibeam antennas. To validate the proposed concept, this paper presents the design of a multibeam lens antenna capable of achieving five beams over a range of $\pm 60°$. Simulation and measured results demonstrate a 3 dB axis ratio bandwidth of 12.6-17.1 GHz, a reflection coefficient of less than -10 dB, and the gain exceeding 21 dBi at 15 GHz.

II. LENS THEORY AND DESIGN

For traditional Luneburg lenses, their equivalent refractive index distribution satisfies the formula [18]:

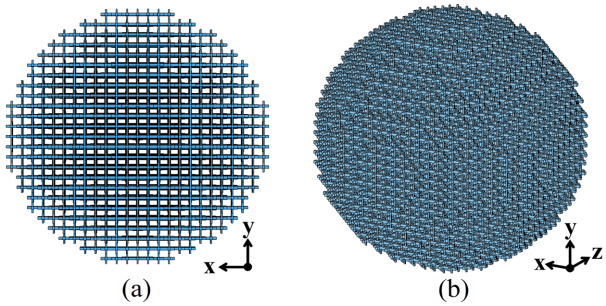

FIGURE 3. Model diagram of the Luneburg lens structure with 13 shells. (a) Side view. (b) Perspective view.

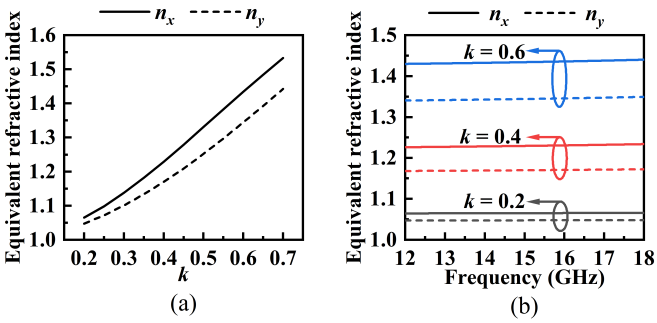

FIGURE 4. Equivalent refractive index of unit cell. (a) As a function of the normalized size k at 15GHz ($k = a/l$). (b) As a function of frequency.

$$n(r) = \sqrt{2 - r^2} \tag{1}$$

where r is the normalized radius and n is the equivalent refractive index. The specific design method of Luneburg lens will be explained in this section.

A. DISCRETE UNIT SETTING

To achieve gradient refractive index, the spherical Luneburg lens is discretized into concentric spherical layers of the same thickness. Then discretize each layer into smaller cells, as shown in Fig. 1. As the number of layers of the Luneburg lens increases, the improvement in its radiation characteristics becomes less significant. Therefore, considering various factors comprehensively, the Luneburg lens in this letter is constructed as a 13 layer structure, with each layer filled with unit cells having corresponding equivalent refractive indices.

The unit cell of the Luneburg lens is shown in Fig. 2, with a size of 4mm $\times$ 4mm $\times$ 4mm ($= \lambda_0/5$ at 15 GHz) to ensure the equivalent dielectric theory. It is composed of three mutually orthogonal dielectric rods, and the equivalent refractive index is controlled by adjusting the size of the dielectric rods. The lens composed of this unit cell is shown in Fig. 3. To achieve different transmission characteristics for x-polarized waves and y-polarized waves incident on the lens, in this paper, the size of the dielectric rod along the y direction is reduced by half. By using electromagnetic waves with different polarizations incident on the unit cells, the equivalent refractive

This work is licensed under a Creative Commons Attribution-NonCommercial-NoDerivatives 4.0 License. For more information, see https://creativecommons.org/licenses/by-nc-nd/4

This article has been accepted for publication in IEEE Access. This is the author's version which has not been fully edited and
content may change prior to final publication. Citation information: DOI 10.1109/ACCESS.2025.3531956

TABLE 1. TOTAL PHASE DIFFERENCES OF DIFFERENT LAYERS

Layers	11	12	13	14
$\triangle\varphi_l$ (deg)	83.5	92.9	100	107.6

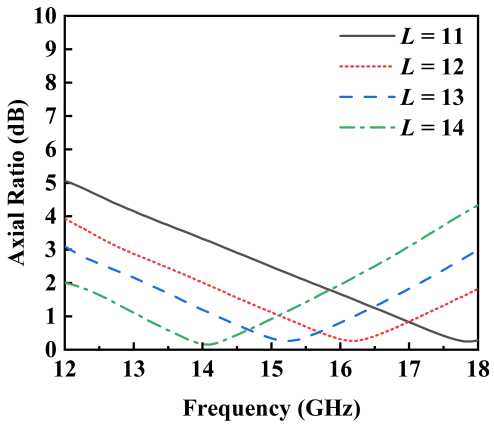

FIGURE 5. Simulated axial ratio (AR) of the different layers Luneburg lens.

indices n_x and n_y for x polarization and y polarization are derived from the S-parameters. The relationship between the equivalent refractive index and the dielectric rod size is shown in Fig. 4(a), which indicates that the size range of unit cells can achieve a change in equivalent refractive index from 1 to $\sqrt{2}$. Fig. 4(b) shows that the unit cell has frequency independent characteristics, which is consistent with the theoretical results.

B. REALIZATION OF CIRCULAR POLARIZATION

Two orthogonal linear polarized waves of the same size and 90° phase difference can be synthesized into a circular polarized wave. Therefore, using a linear polarized antenna with a polarization angle of 45° from the x-axis as the feed source, the linear polarization can be decomposed into an x-polarization and a y-polarization. When two equivalent polarized electromagnetic waves pass through a certain unit cell, they will produce different phase shifts φ_x and φ_y. The phase difference $\triangle\varphi$ of a single unit cell between φ_x and φ_y is determined by [36]

$$\triangle\varphi = \varphi_x - \varphi_y = 2\pi \cdot (n_x - n_y) \cdot \frac{l}{\lambda_0} \tag{2}$$

where λ_0 is the free-space wavelength and l is the size of the discrete unit. It can be seen that $\triangle\varphi$ is determined by the size of the dielectric rod l from (2). Therefore, it is only necessary to control the two polarized electromagnetic waves to produce a 90° phase difference when passing through the whole Luneburg lens, which can achieve the transformation of linear polarized waves into circular polarized waves, that is, the phase difference $\triangle\varphi_l$ of total lens can be calculated by [36]

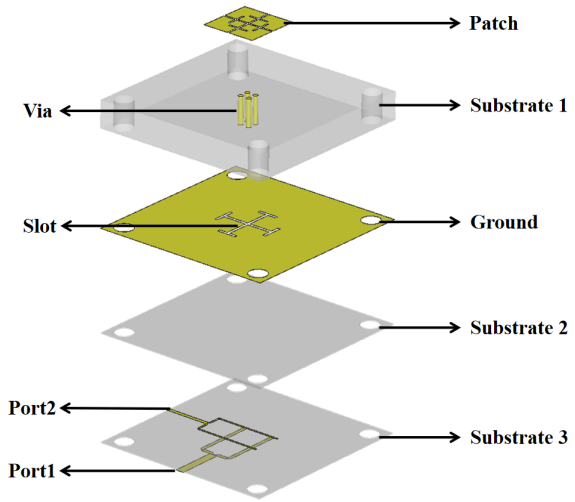

FIGURE 6. The 3D view and layer information of the feeding antenna.

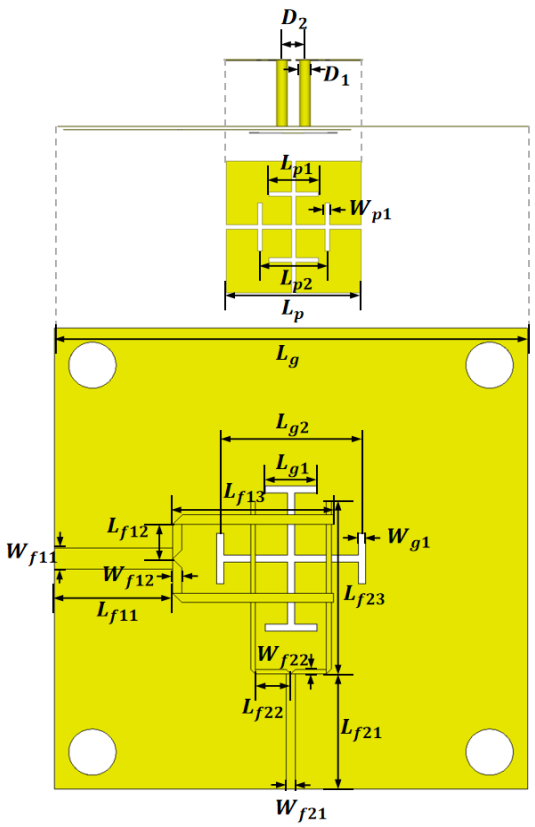

FIGURE 7. The dimension details of ME dipole antenna.

$$\triangle\varphi_l = \sum_{i=1}^{N} 2\pi \cdot (n_{x_i} - n_{y_i}) \cdot \frac{l}{\lambda_0} = 90° \tag{3}$$

where N is the number of unit cells through which the incident wave passes, n_{x_i} and n_{y_i} are the equivalent refractive indices of the ith unit cell, and λ_0 is the free space wavelength at 15

This work is licensed under a Creative Commons Attribution-NonCommercial-NoDerivatives 4.0 License. For more information, see https://creativecommons.org/licenses/by-nc-nd/4

This article has been accepted for publication in IEEE Access. This is the author's version which has not been fully edited and content may change prior to final publication. Citation information: DOI 10.1109/ACCESS.2025.3531956

TABLE 2. THE DIMENSION DETAILS OF ME DIPOLE ANTENNA

Length	L_g	L_p	D_1	D_2	L_{g1}	L_{g2}
Value (mm)	20	6	0.5	1	2.2	6
Length	W_g	L_{p1}	L_{p2}	W_{p1}	W_{f11}	W_{f12}
Value (mm)	0.3	2.2	3	0.2	0.9	0.4
Length	L_{f11}	L_{f12}	L_{f13}	W_{f21}	W_{f22}	
Value (mm)	5	1.5	6.8	0.4	0.2	

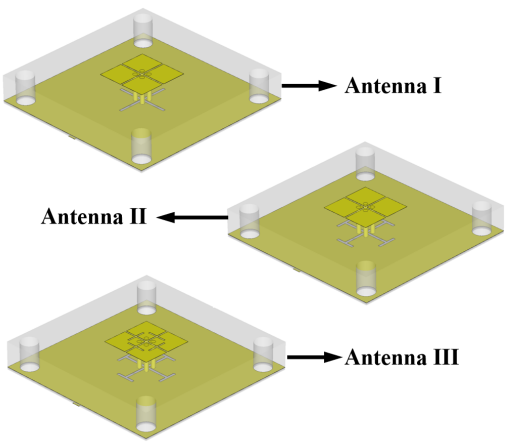

FIGURE 8. Antenna I: Original model. Antenna II: Using an "I" shaped coupling gap. Antenna III: Slotting on radiation patch.

GHz. Then, the total phase difference of different layers can be calculated from (3), as shown in Table 1.

In order to verify the calculation results, the Luneburg lens of different layers models were established, and the dipole antenna has 45° rotation relative to the Luneburg lens were used as the feed source. The simulated axial ratio (AR) values are shown in Fig. 5. It can be seen that the 13 layer Luneburg lens has a better 3 dB AR bandwidth at the Ku-band, so this letter chooses the 13 layer lens for further study.

III. DESIGN OF THE MULTIBEAM ANTENNA

A. DESIGN OF FEED ANTENNA

The section presents a dual-polarized magneto-electric (ME) dipole antenna to provide two linear polarized waves. The ME dipole consists of three pieces of Rogers RT5880 radiation medium with a dielectric constant of 2.2 and a loss tangent of 0.0009. The ME dipole radiation structure of the patch loaded symmetric etching gap studied in this section is shown in Fig. 6. Four horizontal metal patches and metal ground are located on the top and bottom layers of the substrate 1, respectively, and are connected through four vertical metal through-holes penetrating the substrate 1. The metal ground is etched with an "I" shaped coupling gap. The feeding networks are located at the bottom of substrate 2 and 3. Two similar feeding networks are orthogonally placed to achieve the dual-polarized operation. The four holes around the antenna are used to secure the antenna. The dimension details of the proposed antenna are shown in Fig. 7 and listed in Table 2.

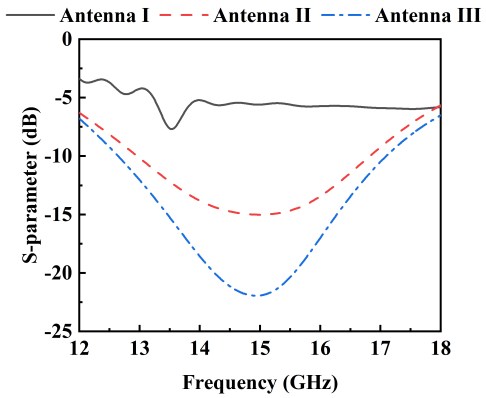

FIGURE 9. The S-parameter of different antennas.

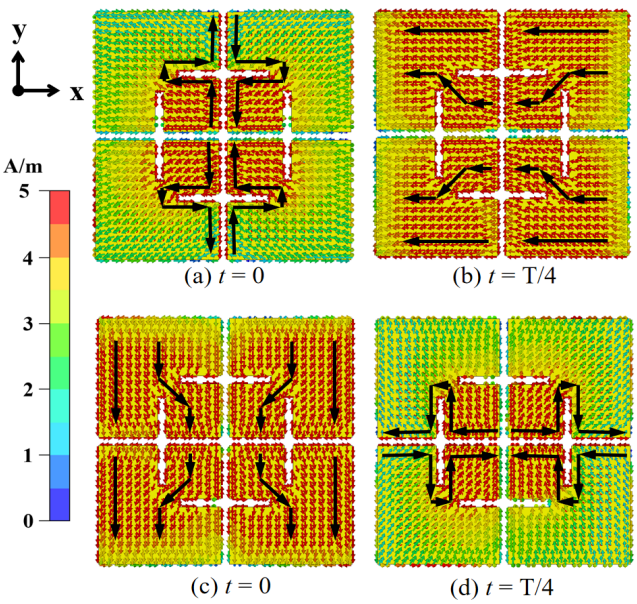

FIGURE 10. The current distribution image for ME dipole antenna. (a)(b)Port1. (b)(c)Port2.

In order to better illustrate how the proposed antenna improves radiation performance, two other reference antennas were studied and compared, as shown in Fig. 8. Antenna III is the antenna proposed in this section, and antenna I is the original model. Compared with antenna I, antenna II adopts an "I" type coupling gap, and antenna III further adds slots on the patch, while keeping other parts unchanged. Fig. 9 shows the S-parameters of three types of antennas. It can be seen that the return loss of antenna I is very high, it is not effectively excited, and antenna III has lower return loss and wider impedance bandwidth compared to antenna I and antenna II.

The current distributions at different time points t = 0 and t = T/4 (where T is the oscillation period of 15GHz) are shown in Fig. 10. Electric dipoles and magnetic dipoles are respectively realized by the patch and the radiation gap between the horizontal metal patch. Among them, the four

This work is licensed under a Creative Commons Attribution-NonCommercial-NoDerivatives 4.0 License. For more information, see https://creativecommons.org/licenses/by-nc-nd/4

This article has been accepted for publication in IEEE Access. This is the author's version which has not been fully edited and
content may change prior to final publication. Citation information: DOI 10.1109/ACCESS.2025.3531956

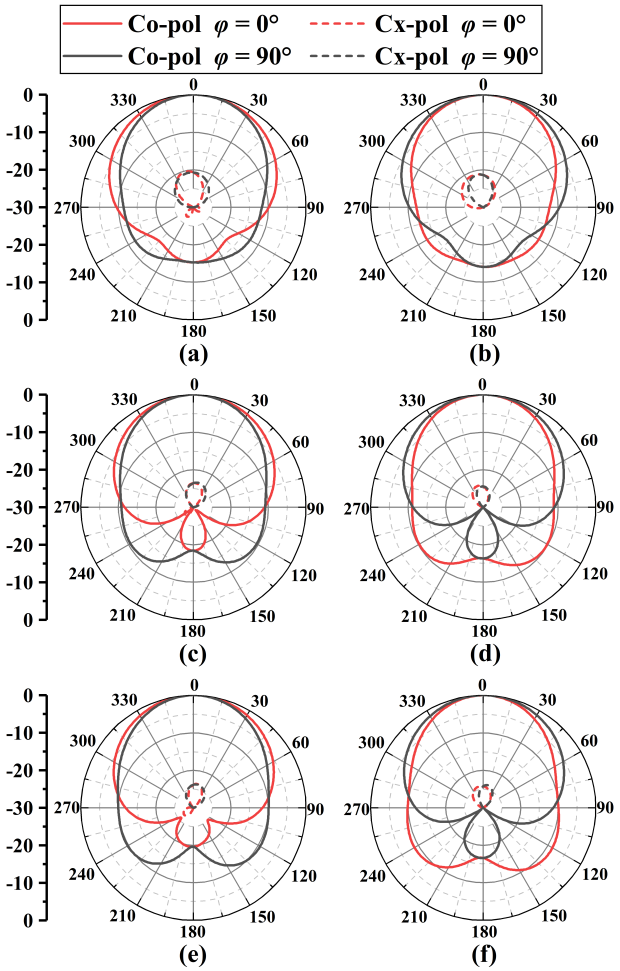

FIGURE 11. Simulated radiation pattern of the antenna at (a)(b) 13, (c)(d) 15, and (e)(f) 17 GHz. (a)(c)(e) Port 1. (b)(d)(f) Port 2.

short circuit horizontal metal patches have the same width and are all quarter wavelength, thus forming two pairs of half wavelength electric dipoles in polarization direction. Since the current distributions at the time points $t = T/2$ and $t = 3T/4$ have the same amplitude but opposite directions to those of $t = 0$ and $t = T/4$, they are not shown here for brevity. With reference to Fig. 10(a)(b), at time $t = 0$, the current density on the planar patches becomes minimum, but the current density on the radiating aperture between patches reaches a maximum, indicating that the magnetic dipole mode is excited. Whereas at time $t = T/4$, the current density on the planar patches reaches a maximum, which means that the electric dipoles are strongly excited. That is to say, the electric dipole mode and the magnetic dipole mode are excited alternatively with 90° phase difference, hence, this antenna operates as an ME dipole antenna. The magnetic dipole is not composed of a traditional vertical short circuited metal column with a wavelength height of one quarter, so the height of the electromagnetic dipole radiation structure is not limited to $0.25\lambda_c$ but it can be as low as $0.16\lambda_c$. Comparing Fig. 10(a)(b) with (c)(d), it can be seen that two orthogonal currents are excited by Port1 and Port2, further generating two mutually orthogonal linearly polarized waves.

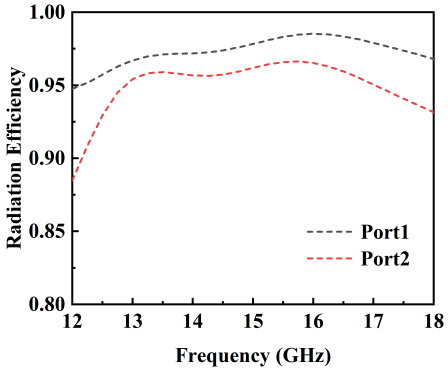

FIGURE 12. The radiation efficiency of antenna III.

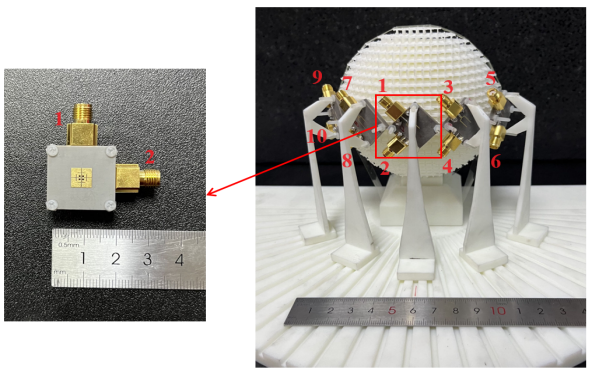

FIGURE 13. Photograph of feeding antenna and Luneburg lens antenna with supporting structure.

Fig. 11 shows the simulated radiation patterns of dual polarization at 13, 15, and 17 GHz. As expected, similar broadside radiation patterns are obtained at both ports. At the boresight direction, the main polarization is more than 20 dB higher than the cross polarization. The antenna radiation efficiency has also been studied and shown in Fig. 12, and satisfactory radiation performance can be observed, which is about 95% within the operating bandwidth.

B. MULTIBEAM LUNEBURG LENS ANTENNA

The proposed multibeam Luneburg Lens Antenna is illustrated in Fig. 13. Five feeding antennas are supported by brackets and cover the Luneburg lens ±60°. The feed antenna rotates 45° relative to the Luneburg lens to generate two 45° linear polarized waves. This multibeam Luneburg lens antenna has ten ports, with symmetrical structures from Port3 to Port6 and from Port7 to Port10. For the convenience of discussion, the following text will only analyze Port1 to Port6.

IV. MEASUREMENT AND DISCUSSION

Impedance characteristics testing was conducted using a vector network analyzer. The reflection coefficient test results

This work is licensed under a Creative Commons Attribution-NonCommercial-NoDerivatives 4.0 License. For more information, see https://creativecommons.org/licenses/by-nc-nd/4

This article has been accepted for publication in IEEE Access. This is the author's version which has not been fully edited and
content may change prior to final publication. Citation information: DOI 10.1109/ACCESS.2025.3531956

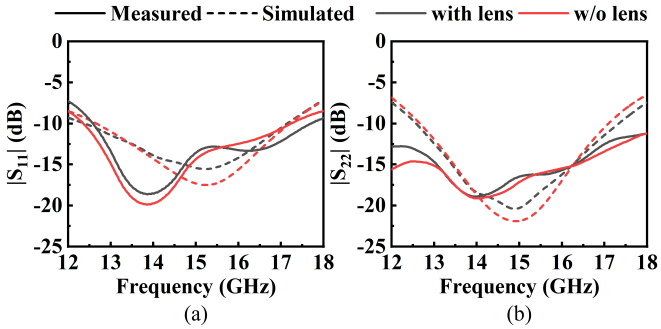

FIGURE 14. Simulated and measured reflection coefficient of the single feeding antenna. (a) Port1. (b) Port2.

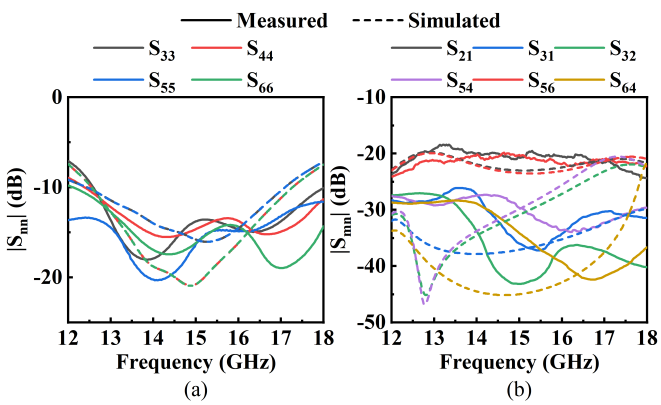

FIGURE 15. Simulated and measured (a) reflection coefficient and (b) mutual coupling of the multibeam antenna.

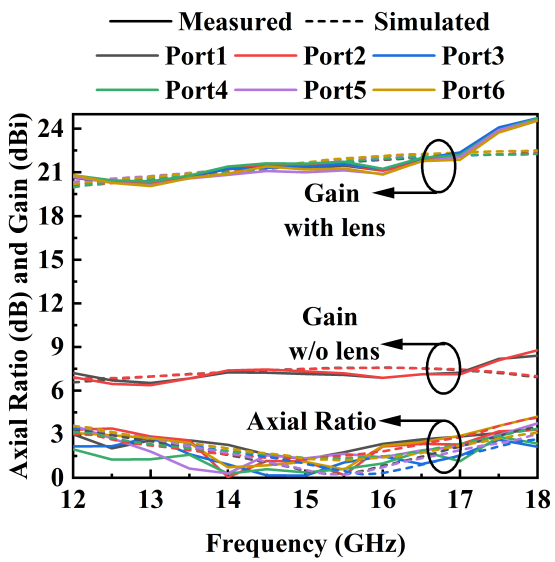

FIGURE 16. Simulated and measured axial ratio and gain of the multibeam antenna.

for the feed antenna are presented in Fig. 14. The results indicate that the presence of the lens has no significant impact on the impedance matching of the feed antenna. A relative

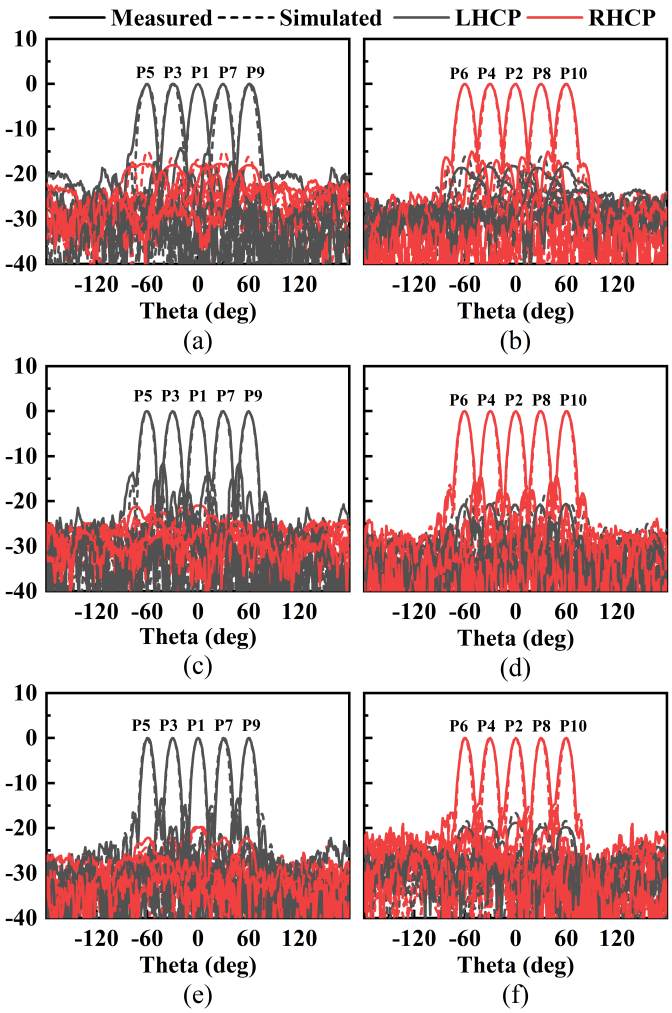

FIGURE 17. Simulated and measured normalized LHCP and RHCP radiation pattern at (a)(b) 13, (c)(d) 15, and (e)(f) 17 GHz.

bandwidth exceeding 33.7% within the range of less than -10 dB has been achieved, covering almost the entire Ku-band. The mutual coupling between different feeds is depicted in Fig. 15. In the Ku-band, the coupling between different ports of the feeding antenna is less than -18.5 dB.

The axial ratio and gain measurements, conducted in a microwave anechoic chamber, are illustrated in Fig. 16. Within the operating frequency range, the axial ratio is less than 3 dB. The gain of the feeding antenna is around 7 dBi. Adding the lens, the gain reaches around 21 dBi. The lens improves the gain of feeding antenna by 14 dB, showing good radiation performances.

Fig. 17 displays the measured radiation pattern and simulated radiation pattern for the multibeam antenna. A total of five beams cover a spatial range of $\pm 60°$. Fig. 17(a)(c)(e) show the left-handed circularly polarized (LHCP) wave fed from Port1, Port3, Port5, Port7, and Port9, while Fig. 13(b)(d)(f) show the right-handed circularly polarized (RHCP) wave fed from Port2, Port4, Port6, Port8, and Port10. The change of LHCP and RHCP modes only requires switch-

This work is licensed under a Creative Commons Attribution-NonCommercial-NoDerivatives 4.0 License. For more information, see https://creativecommons.org/licenses/by-nc-nd/4

This article has been accepted for publication in IEEE Access. This is the author's version which has not been fully edited and
content may change prior to final publication. Citation information: DOI 10.1109/ACCESS.2025.3531956

TABLE 3. COMPARISON WITH REPORTED MULTIBEAM LUNEBURG LENS ANTENNAS

Ref.	Dimension	Lens Type	BW(%) @(GHz)	Polarization	Gain (dBi)
[22]	2D	3DP PPW Metal nail	42.8@140	LP	20
[23]	2D	3DP PPW Dielectric rods	43@26.75	LP to CP	10
[25]	2D	3DP PPW Air hole	13.3@15	Dual LP	14.7
[29]	2D	3DP DSW Air hole	23.5@10	LP to CP	13.7
[31]	3D	3DP Dielectric lens	40@33	LP	21.2
[32]	3D	3DP Dielectric lens	n.a.@110	LP	21.3
[34]	3D	3DP Dielectric lens	31.6@10	LP to CP	13.8
This work	3D	3DP Dielectric lens	30@15	Dual LP to Dual CP	21

ing the port of the feed antenna, without the mechanical operation. The simulation results align closely with the measurement results.

Table 3 presents a comparison between the proposed multibeam Luneburg lens antenna and the previously reported ones. It is noted that each of the reported antennas possesses its own unique merits. The antenna proposed in this paper offers the advantage of being easily manufacturable by 3DP, while also exhibiting a stable geometric configuration. This lens antenna not only fulfills the functions of traditional Luneburg lens but also serves as a polarizer, enabling the conversion of dual linear polarized waves into dual circularly polarized waves. It further features a broad 3 dB AR bandwidth and a high gain. Moreover, the polarization mode can be easily changed by switching the ports of the feeding antenna, instead of mechanical rotation.

V. CONCLUSION

A 3D-printed wideband multibeam dual circularly polarized Luneburg lens antenna in the Ku-band has been proposed and fabricated in this paper. The proposed Luneburg lens serves not only classical Luneburg lens but also a polarizer to transform the dual-linear polarization incident wave to dual-circular polarization wave. Polarization conversion was achieved using asymmetric unit cells. This paper is the first to achieve spherical dual-circular polarized Luneburg lens by simply switching the ports of the feeding antenna without the need for mechanical rotation or replacement of the feeding antenna. This is a reliable method to change the polarization mode without causing additional errors. Five dual-linear polarized ME dipole antennas as feed achieve dual-circular polarization multibeam coverage within a $\pm 60^\circ$ range. Five LHCP and five RHCP beams with gains of 20.1-22.4 dBi and broad bandwidth up to 30% (12.6 GHz–17.1 GHz) are achieved in terms of reflection coefficients lower than -10 dB and axial ratios smaller than 3 dB. The measured and simulated results agree well. The proposed low-cost multibeam antenna has application value in fields such as military, mobile, and satellite communication.

REFERENCES

[1] W. Hong, Z. H. Jiang, C. Yu, J. Zhou, P. Chen, Yu *et al.*, "Multibeam antenna technologies for 5g wireless communications," *IEEE Trans. Antennas Propag.*, vol. 65, no. 12, pp. 6231–6249, 2017.

[2] B. Nie, H. Lu, T. Skaik, Y. Liu, and Y. Wang, "A 3d-printed subterahertz metallic surface-wave luneburg lens multibeam antenna," *IEEE Trans. Terahertz Sci. Technol.*, vol. 13, no. 3, pp. 297–301, 2023.

[3] Y. J. Guo, M. Ansari, R. W. Ziolkowski, and N. J. G. Fonseca, "Quasi-optical multi-beam antenna technologies for b5g and 6g mmwave and thz networks: A review," *IEEE Open J. Antennas Propag.*, vol. 2, pp. 807–830, 2021.

[4] M. Ansari, B. Jones, and Y. Jay Guo, "A wide angle scanning spherical luneburg lens antenna employing metamaterial," in *Proc. IEEE Int. Symp. Antennas Propag. (APSURSI)*, 2022, pp. 1632–1633.

[5] G. Yang, Y. Zhang, and S. Zhang, "Wide-band and wide-angle scanning phased array antenna for mobile communication system," *IEEE Open J. Antennas Propag.*, vol. 2, pp. 203–212, 2021.

[6] J. G. Marin and J. Hesselbarth, "Lens antenna with planar focal surface for wide-angle beam-steering application," *IEEE Trans. Antennas Propag.*, vol. 67, no. 4, pp. 2757–2762, 2019.

[7] Y. Lu, J. Li, J. Qin, S. Chen, and T. Yuan, "A compact and monolithically 3-d printed millimeter-wave high-gain horn antenna," in *Proc. 2023 Asia-Pacific Microw. Conf. (APMC)*, 2023, pp. 839–841.

[8] M. Liang, W.-R. Ng, K. Chang, K. Gbele, M. E. Gehm, and H. Xin, "A 3-d luneburg lens antenna fabricated by polymer jetting rapid prototyping," *IEEE Trans. Antennas Propag.*, vol. 62, no. 4, pp. 1799–1807, 2014.

[9] G. Guo, Y. Xia, C. Wang, M. Nasir, and Q. Zhu, "Optimal radiation pattern of feed of luneburg lens for high-gain application," *IEEE Trans. Antennas Propag.*, vol. 68, no. 12, pp. 8139–8143, 2020.

[10] A. Alkhateeb, J. Mo, N. Gonzalez-Prelcic, and R. W. Heath, "Mimo precoding and combining solutions for millimeter-wave systems," *IEEE Commun. Mag.*, vol. 52, no. 12, pp. 122–131, 2014.

[11] J. D. Díaz, J. L. Salazar-Cerreno, J. A. Ortiz, N. A. Aboserwal, R. M. Lebrón, C. Fulton, and R. D. Palmer, "A cross-stacked radiating antenna with enhanced scanning performance for digital beamforming multifunction phased-array radars," *IEEE Trans. Antennas Propag.*, vol. 66, no. 10, pp. 5258–5267, 2018.

[12] A. N. Plastikov, "A high-gain multibeam bifocal reflector antenna with 40° field of view for satellite ground station applications," *IEEE Trans. Antennas Propag.*, vol. 64, no. 7, pp. 3251–3254, 2016.

[13] S. G. Hay, S. L. Smith, G. P. Timms, and J. W. Archer, "Three-shaped-reflector beam-scanning pillbox antenna suitable for mm wavelengths," *IEEE Trans. Antennas Propag.*, vol. 59, no. 7, pp. 2495–2501, 2011.

[14] K. Trzebiatowski, W. Kalista, M. Rzymowski, L. Kulas, and K. Nyka, "Multibeam antenna for ka-band cubesat connectivity using 3-d printed lens and antenna array," *IEEE Antennas Wireless Propag. Lett.*, vol. 21, no. 11, pp. 2244–2248, 2022.

[15] G. H. Lee, S. Kumar, H. C. Choi, and K. W. Kim, "Wideband high-gain double-sided dielectric lens integrated with a dual-bowtie antenna," *IEEE Antennas Wireless Propag. Lett.*, vol. 20, no. 3, pp. 293–297, 2021.

[16] A. Raeesi, A. Palizban, A. Ehsandar, H. Al-Saedi, S. Gigoyan, W. M. Abdel-Wahab, and S. Safavi-Naeini, "A low-profile 2d passive phased-array antenna-in-package for emerging millimeter-wave applications," *IEEE Transactions on Antennas and Propagation*, vol. 71, no. 1, pp. 1093–1098, 2023.

[17] W. Li, H. Tu, Y. He, L. Zhang, S. W. Wong, and S. Gao, "A novel wideband tightly coupled dual-polarized reflectarray antenna," *IEEE Transactions on Antennas and Propagation*, 2023.

[18] R. K. Luneburg, E. Wolf, and M. Herzberger, *Mathematical Theory of Optics*. Math. Theory Opt., 1964.

[19] B. Fuchs, L. Le Coq, O. Lafond, S. Rondineau, and M. Himdi, "Design optimization of multishell luneburg lenses," *IEEE Trans. Antennas Propag.*, vol. 55, no. 2, pp. 283–289, 2007.

[20] S. Morgan, "Generalizations of spherically symmetric lenses," *IRE Trans. Antennas Propag.*, vol. 7, no. 4, pp. 342–345, 1959.

[21] H. T. Chou, Y. S. Chang, H. J. Huang, Z. D. Yan, T. Lertwiriyaprapa, and D. Torrungrueng, "Optimization of three-dimensional multi-shell dielectric lens antennas to radiate multiple shaped beams for cellular radio coverage," *IEEE Access*, vol. 7, pp. 182 974–182 982, 2019.

This work is licensed under a Creative Commons Attribution-NonCommercial-NoDerivatives 4.0 License. For more information, see https://creativecommons.org/licenses/by-nc-nd/4

This article has been accepted for publication in IEEE Access. This is the author's version which has not been fully edited and
content may change prior to final publication. Citation information: DOI 10.1109/ACCESS.2025.3531956

[22] W. Yu, X. Wang, H. Lu, H. Liu, and C. Jin, "3d-printed all-metal terahertz multibeam lens antenna based on photonic crystal," *IEEE Access*, vol. 11, pp. 41 609–41 617, 2023.
[23] C. Wang, J. Wu, and Y.-X. Guo, "A 3-d-printed wideband circularly polarized parallel-plate luneburg lens antenna," *IEEE Trans. Antennas Propag.*, vol. 68, no. 6, pp. 4944–4949, 2020.
[24] O. Zetterstrom, R. Hamarneh, and O. Quevedo-Teruel, "Experimental validation of a metasurface luneburg lens antenna implemented with glide-symmetric substrate-integrated holes," *IEEE Antennas Wireless Propag. Lett.*, vol. 20, no. 5, pp. 698–702, 2021.
[25] B. Qu, S. Yan, A. Zhang, F. Wang, and Z. Xu, "3-d printed cylindrical luneburg lens for dual polarization," *IEEE Antennas Wireless Propag. Lett.*, vol. 20, no. 6, pp. 878–882, 2021.
[26] F. Fan, M. Cai, J. Zhang, Z. Yan, and J. Wu, "Wideband low-profile luneburg lens based on a glide-symmetric metasurface," *IEEE Access*, vol. PP, no. 99, pp. 1–1, 2020.
[27] B. Hu, T. Wu, Y. Cai, W. Zhang, and B. L. Zhang, "A novel metamaterial-based planar integrated luneburg lens antenna with wide bandwidth and high gain," *IEEE Access*, vol. 8, pp. 4708–4713, 2020.
[28] V. Kaschten, D. Lederer, and C. Craeye, "A cylindrical mismatched luneburg lens implemented on pcb at v-band," in *Proc. 18th Eur. Conf. Antennas Propag. (EuCAP)*, 2024, pp. 1–5.
[29] S. Lei, G. Wei, K. Han, X. Li, and T. Qiu, "A wideband 3-d-printed multibeam circularly polarized ultrathin dielectric slab waveguide luneburg lens antenna," *IEEE Antennas Wireless Propag. Lett.*, vol. 21, no. 8, pp. 1582–1586, 2022.
[30] H. C. Chou, N.-L. Tung, and M. N. M. Kehn, "The double-focus generalized luneburg lens design and synthesis using metasurfaces," *IEEE Trans. Antennas Propag.*, vol. 66, no. 9, pp. 4936–4941, 2018.
[31] Y. Li, L. Ge, M. Chen, Z. Zhang, Z. Li, and J. Wang, "Multibeam 3-d-printed luneburg lens fed by magnetoelectric dipole antennas for millimeter-wave mimo applications," *IEEE Trans. Antennas Propag.*, vol. 67, no. 5, pp. 2923–2933, 2019.
[32] F. Meng, Y. Guo, K. Ma, and Y. Luo, "A terahertz wide-angle beamsteering 3-d printed half-compressed elliptical luneburg lens with planar focal plane," *IEEE Antennas Wireless Propag. Lett.*, vol. 23, no. 2, pp. 843–847, 2024.
[33] H. F. Ma and T. J. Cui, "Three-dimensional broadband and broad-angle transformation-optics lens," *Nature communications*, vol. 1, no. 1, p. 124, 2010.
[34] S. Lei, G. Wei, K. Han, X. Li, and T. Qiu, "A simple method to design wideband circularly polarized spherical multibeam luneburg lens antenna," *IEEE Antennas Wireless Propag. Lett.*, vol. 21, no. 7, pp. 1423–1427, 2022.
[35] H. Kirschbaum and S. Chen, "A method of producing broad-band circular polarization employing an anisotropic dielectric," *IRE Trans. Microw. Theory Tech.*, vol. 5, no. 3, pp. 199–203, 1957.
[36] K. X. Wang and H. Wong, "Design of a wideband circularly polarized millimeter-wave antenna with an extended hemispherical lens," *IEEE Trans. Antennas Propag.*, vol. 66, no. 8, pp. 4303–4308, 2018.

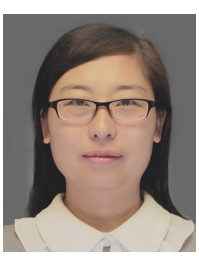

QING WANG was born in Shaanxi, China, in 1984. She received the B.Eng. degree in Measuring and Control Technology and Instrumentations from Xidian University, China, in 2006 and Ph.D. degree in Electromagnetic Field and Microwave Technology from Xidian University, China, in 2012. From 2009 to 2011, she was a visiting student in Clemson University, USA. She is currently an Assistant Professor with the School of Electronic Engineering, Xidian University, Xi'an. Her research interests include lens antenna, topological photonic crystals, terahertz technology, computational electromagnetics, etc.

XIAOHAI HAN was born in Shaanxi, China. He received the B.S. degree in electronics and information engineering from the Xidian University, Xi'an, China, in 2022, where he is currently pursuing the M.S. degree in electromagnetic field and microwave technology. His current research interests include 3D-printed Luneburg lens and millimeter-wave antennas.

PU YU was born in Shaanxi, China. She received the B.Eng. degree in optoelectronic information science and engineering from Nangjing University of Posts and Telecommunications, Nanjing, China, in 2019, and the M.S. degree in Electronics and Communications Engineering from Xidian University, Xi'an, China, in2022. She is currently an antenna engineer with Shaanxi Changling Electronic Technology Co., Ltd, Xi'an. Her current research interests include Wireless Terminal Antenna, Luneburg lens antennas, and millimeter-wave antennas.

JIAN-QIANG HOU received the B.Eng. degree in electromagnetic field and microwave technology from Xidian University, China, in 1999, M.E. degree in electromagnetic field and microwave technology from Xidian University, China, in 2004 and Ph. D. degree in electromagnetic field and microwave technology from Xidian University, China, in 2012.

He is currently an associate Professor with the School of Electronic Engineering, Xidian University, Xi'an. His research interest contains microwave millimeter-wave circuits and systems and modeling and design of microwave devices and optoelectronic devices.

ZHEN-YA LEI was born in Shaanxi, China in 1960. He received the B.Eng. degree in computer science from Xidian University, China, in 1981 and M.E. degree in electromagnetic field and microwave technology from Xidian University, China, in 1998. He was a visiting scholar in Ohio State University, U.S. in 2016.

He is currently a Professor with the School of Electronic Engineering, Xidian University, Xi'an. His research interest contains microwave circuits and microwave engineering, Rf/microwave transmitter and the receiver, antenna, system-level EM field analysis, target characteristics and stealth design.

This work is licensed under a Creative Commons Attribution-NonCommercial-NoDerivatives 4.0 License. For more information, see https://creativecommons.org/licenses/by-nc-nd/4